THE JOURNAL OF PHYSICAL CHEMISTRY C

pubs.acs.org/JPCC Article

Solvation and Stabilization of Single-Strand RNA at the Air/Ice Interface Support a Primordial RNA World on Ice

Ivan Gladich,* Margaret L. Berrens, Penny M. Rowe, Rodolfo G. Pereyra, and Steven Neshyba*

Cite This: https://dx.doi.org/10.1021/acs.jpcc.0c04273 Read Online

ACCESS | Metrics & More | Article Recommendations | Supporting Information

ABSTRACT: Outstanding questions about the RNA world hypothesis for the emergence of life on Earth concern the stability and self-replication of prebiotic aqueous RNA. A recent experimental work has suggested that solid substrates and low temperatures could help resolve these issues. Herein, we use classical molecular dynamics simulations to explore the possibility that the substrate is ice itself. Simulations at −20 °C show that an eight-nucleotide single strand of RNA, initially situated in the quasiliquid layer at the air/ice interface, exhibits a robust propensity to reorient itself—its bases turn toward the (hydrophobic) air/ice interface, while its anionic phosphodiester oxygens align with the underlying ice lattice. Kinetic analysis of hydrogen bonding indicates resistance to hydrolysis that is greater than that of an aqueous single-strand RNA at the same temperature. This enhanced resistance, in turn, could increase the opportunities for polymerization and self-copying. These findings thus offer the possibility of a role for an ancient RNA world on ice distinct from that considered in extant elaborations of the RNA world hypothesis. This work is, to the best of our knowledge, the first molecular dynamics study of RNA on ice.

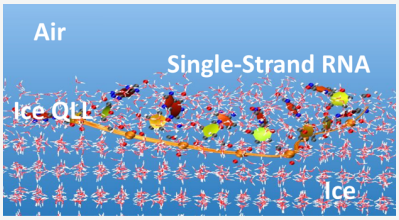

INTRODUCTION

According to the *RNA world* hypothesis, terrestrial life began with the formation of polymeric chains of ribonucleic acid (RNA) in a prebiotic soup of complex organic molecules.[1−9] In this hypothesis, chains of RNA, rather than DNA, were the first informational polymer[3−5] and catalyzed their own polymeric growth and replication by Watson−Crick base-pairing,[6] evolving toward more complex molecular machineries up to the first cellular life. Prior works supporting this hypothesis include the observations that some forms of RNA (i.e., ribozymes) are capable of biocatalytic activity,[7−10] and that in modern life the assembly of amino acids into protein chains in the ribosome of all living cells is catalyzed by ribosomal RNA. Moreover, RNA fragments are attached to various enzymatic cofactors, which are widely interpreted as a vestige of an ancient RNA world.[11]

Unresolved questions remain, however, about the emergence of prebiotic RNA and its evolution in the absence of protein-assisted biochemical mechanisms. Even granting abiotic formation of nucleotides in a prebiotic soup (a topic still intensely debated[6,11−14]), polymerization of nucleotides faces an uphill free energy gradient.[11] In addition, in an aqueous solution at room temperature, RNA polynucleotides degrade quickly[15] because the phosphodiester link between monomers is vulnerable to nucleophilic attack and breakage by the deprotonated 2′-OH group of the ribose sugar.[16,17] Experimental investigations have (so far) shown that the synthesis of complementary RNA strands, by template-directed synthesis from pre-existing RNA chains or catalyzed by other short RNA chains acting as a replicase ribozyme, is slow compared to hydrolysis.[18−20]

Recently, two experimental findings have revitalized the RNA world hypothesis. In 2011, Deck et al.[21] observed the growth of an RNA complementary strand from an immobilized RNA template on iron oxide beads in the presence of a solution of free nucleotides and at a low temperature (−20 °C). Subsequently, Attwater et al.[22] were able to design, for the first time, a polymerase ribozyme capable of catalyzing the synthesis of an RNA sequence longer than itself in a subzero saline aqueous solution at −19 °C. Interestingly, this catalytic activity was reported to occur in the eutectic phase at the interface of two growing ice crystals. Before this, in vitro ribozymes never accomplished the synthesis of RNA strands of their own size.[22]

These findings point to the possibility of ice as a key substrate for a cold start for life. Within this context, a number of physicochemical insights into aqueous solute behaviors at the air/ice interface come into view. First, the exposed part of air/condensed water interfaces has been shown to be a preferential environment for the (partial) solvation of organic molecules containing large nonpolar groups.[23,24] One can expect the hydrophobic base moieties of RNA to behave similarly. Second, at temperatures above ∼200 K, the surface layer of water at an air/ice interface forms a thin, disordered

Received: May 12, 2020
Revised: July 26, 2020
Published: July 28, 2020

("premelted") quasiliquid layer (QLL).[25,26] A growing number of experimental and computational studies[27−34] indicate that this QLL offers conditions that are quite different from those experienced by solutes dissolved in bulk water, namely, a heterogeneous solvation environment comprising the gas phase, the disordered water layer, and the highly structured underlying ice lattice. One can expect that RNA solvated within this highly variegated environment might respond in ways that could not occur in bulk aqueous solutions. Third, phosphate is known to be a strong ionic kosmotrope, that is, it directs, polarizes, and strengthens hydrogen bonding between the nearby water molecules.[35,36] Recent experimental[37] and computational[38] works have indicated that the inner hydration shell of phosphate typically consists of three water molecules hydrogen bonded to each anionic phosphate oxygen (hence, phosphate has an average of ∼12 water molecules in its inner solvation shell). If the anionic oxygens belonging to RNA's phosphodiesters behaved similarly, one would anticipate similar strong interactions with water with the interesting distinction that the ice-like water available for hydrogen bonding at the air/ice interface could impose structural constraints on the RNA that do not occur in aqueous RNA.

To explore whether an ice substrate could play a role in an RNA world, a detailed molecular understanding of the solvation and dynamics of RNA strands on ice is needed. One attractive option for doing so is to employ the tools of molecular dynamics (MD). In this work, we use MD simulations to investigate the behavior of an eight-nucleotide, CCUUCGGG, single-strand RNA sequence on the surface of ice. Short strands such as this are attractive because sampling of different configurations is more affordable on an MD time scale; indeed, this sequence was the subject of prior MD investigations[39,40] in bulk water at 300 K. We find that this approach yields structural and kinetic results that integrate well with (and expand upon) the above-mentioned prior work in bulk liquid water, beginning with the key observation that the air/ice interfacial environment has a distinctive impact on the orientation of RNA solvated at the air/ice interface.

METHODS

MD simulations were performed to investigate the solvation and dynamics of a small (8-nucleotide) single-strand RNA on ice and liquid water. Interaction parameters were adopted from a new force field for nucleic acids and proteins recently proposed by Shaw's group,[41,42] which is provided with the TIP4P-D water model.[43] TIP4P-D is a slight variation of the TIP4P/2005[44] water model, which is one of the most commonly used water models for ice and supercooled liquid water.[45] TIP4P-D adopts the same geometry as TIP4P/2005, slightly modifying the partial charges on atoms and nonbonded interaction parameters. The melting temperature, T_m, of TIP4P/2005 is 252 K.[46] The T_m of TIP4P-D has never been calculated before; in this work, we determined it to be 249 K (see Figures S1 and S2 in the Supporting Information).

An initial proton disordered ice I_h crystal of dimension ∼5.5 nm × 5.5 nm × 4.1 nm (12 bilayers in the z-direction, with a total of 4032 water molecules) was constructed using the Buch algorithm.[47] This ice crystal was annealed from 0 to 229 K (the latter corresponding to T_m—20 K) by performing a 1 ns constant pressure simulation (*NPT*) at 0 bar with a time step of 0.1 fs, followed by another 400 ps at the target temperature. This annealing process allows the dimensions of the ice block to adjust to the increasing temperature. Afterward, the simulation box was enlarged along the z dimension to 16 nm giving rise to an ice slab with two vapor-exposed basal ice facets. Finally, another 2 ns constant volume (*NVT*) simulation was performed, resulting in the formation of two equilibrated interfacial premelted layers. Similar protocols for the preparation of ice slab simulations have been exploited successfully in the literature.[48−50] In this paper, we refer to the above premelted layer as the "ice-QLL layer", and the interface at which it occurs as the "air/ice interface". This nomenclature highlights the fact that the properties of the ice-QLL layer differ from those of supercooled liquid water. Figure S2 in the Supporting Information displays a snapshot at 248 K, showing the ice crystal wetted by the ice-QLL layers at the upper and lower air/ice interfaces.

For the simulation of the single-strand RNA in bulk liquid water, the RNA was solvated in a cubic box of liquid water of a lateral dimension of ∼7 nm (11,126 water molecules) after which the system was equilibrated at a desired temperature of 229 or 274 K, that is, 20 K below and 25 K above the melting temperature of the TIP4P-D water model, respectively. The equilibration was achieved during the course of 1 ns *NPT* simulation at 1 bar pressure. Finally, a production run of 700 ns was achieved in a constant volume and temperature (*NVT*) ensemble.

At room temperature, the CCUUCGGG sequence can fold, forming a tetraloop structure by base pairing of the first and last two nucleotides of the sequence. Bottaro et al.[39] and Cesari et al.[40] have provided an accurate description of the free energy landscape of folding and unfolding of CCUUCGGG at 300 K in bulk water. However, Bottaro et al.[39] and Cesari et al.[40] used a different force field and water model (TIP3P), which are not suitable for ice simulation.[45] The initial structure of CCUUCGGG was generated using the Make-NA web server (http://structure.usc.edu/make-na/server.html) and initially minimized in vacuum before solvating it on ice or supercooled liquid water.

To identify the most probable CCUUCGGG configurations on ice, MD simulations were complemented with an enhanced sampling method (well-tempered metadynamics, hereafter MTD)[51] designed to explore different structural arrangements of the RNA at the air/ice interface and in bulk water. A short (100 ps) *NVT* run with a time step of 0.1 fs was performed to relax the structure after placing the RNA on the ice interface. Afterward, ∼400 ns MTD runs in the *NVT* ensemble, using a time step of 2 fs, were exploited by biasing the end-to-end C1′−C1′ distance, $d_{C1'-C1'}$, of the RNA, depositing a Gaussian potential of 0.1 nm width and a height of 1 kJ/mol every 1000 steps. A bias factor of 300 was adopted. Similarly, we also exploited an MTD run for the single-strand RNA solvated in bulk water at 274 K, that is, 25 K above the melting temperature of the TIP4P-D water model, using a bias factor of 40. For the MTD run on ice (in bulk water), the heights of the Gaussian hills dropped below 0.2 kJ/mol in ∼260 ns (50 ns), with diffuse behavior of the collective variable.[52] Error bars on the free energy profile were of the order of 2 kJ/mol and were calculated according to the method reported in ref 52. The obtained free energy profiles were used to determine the structural global free energy minimum for the RNA on ice. A temperature of 229 K was selected for our runs on the air/basal surface of ice. This temperature corresponds to 20 °C below the melting point of the TIP4P-D water model used here for the classical MD (following the experimental works of Deck et

https://dx.doi.org/10.1021/acs.jpcc.0c04273
J. Phys. Chem. C XXXX, XXX, XXX−XXX

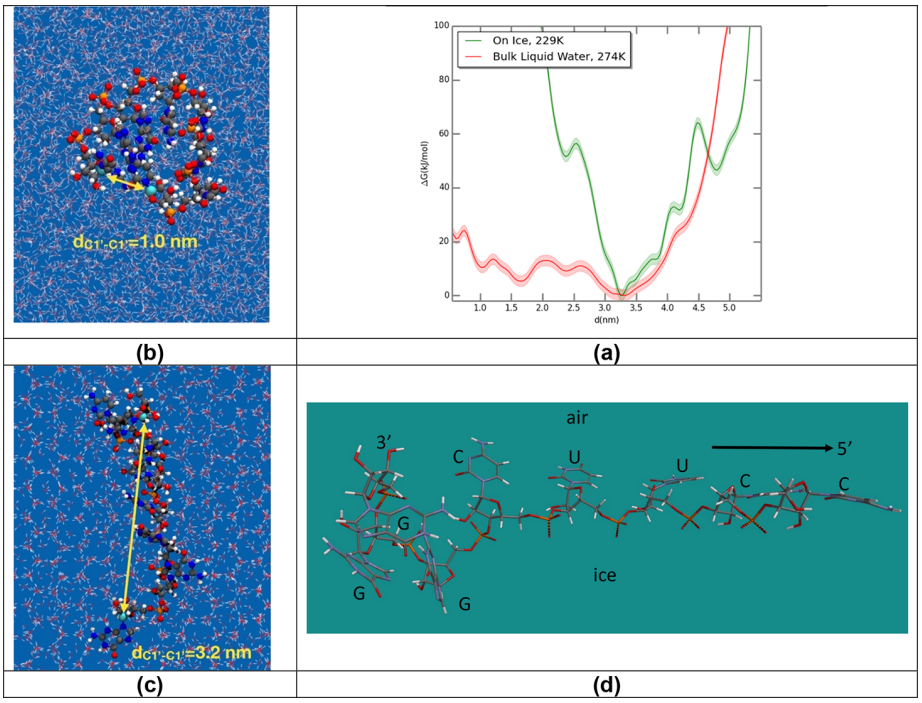

Figure 1. (a) Free energy profiles as a function of the C1′−C1′ end-to-end distance for CCUUCGGG single-strand RNA on the basal surface of ice at 229 K (solid green line) and in bulk water at 274 K (solid red and blue lines, respectively). The methodology for assigning error bars to free energy profiles obtained by metadynamics is still an open question in the community:[52,80,81] here, we have followed the approach in ref 52 and the shadow region in the figure represents three standard deviations (∼2 kJ/mol). (b,c) Top view of representative structures in liquid water and on the air/basal-ice surface, respectively, at $d_{C1'-C1'} \sim 1$ nm (in liquid water) and $d_{C1'-C1'} \sim 3.2$ nm (on ice). (d) Profile view of (c).

al.[21] and Attwater et al.[22]). The initial structures used for the MTD runs are included in the Supporting Information.

As already pointed out in the literature,[39,53,54] even at room temperatures and with single strands of eight nucleotides, simulations of hundreds of microseconds are needed to properly sample the conformational changes among different RNA structures and, at the same time, to provide a quantitative description of the free energy differences among those structures. This becomes even more challenging at low temperatures considered in this work, where the dynamics are much slower. For this reason, to probe the robustness of our free energy profiles, we also performed an unbiased (i.e., without any driving potential) 1 μs MD simulation for the RNA on ice using as the starting condition a configuration with $d_{C1'-C1'} \sim 4.4$ nm, that is, slightly stretched out from the value at the global minimum. After ∼460 ns, the RNA structure on the basal air/ice interface converges to its global minimum at $d_{C1'-C1'} \sim 3.2$ nm (Figure S3a). This supports the reliability of the free energy profile obtained here as a qualitative assessment of the global and local minima of different RNA structures on ice.

In addition, during the MTD runs, we also tracked eRMSD metrics[55] for the system (Figure S4). The eRMSD is a metric based on the difference in the orientation and position of the nucleobases between two RNA structures. This metric has been proven to provide a more reliable description of RNA structures compared to the standard rmsd metrics[39,55] and to be capable of discriminating between RNA structures with and without base pairing.[39] The native reference structure for the eRMSD metric was the CCUUCGGG strand in its tetraloop arrangement taken from the PDB structure 1FTY, residues 7−14. The default cutoff value of 2.4 for eRMSD was adopted.

All simulations were performed using GROMACS 2018.6,[56] employing the leap-frog integration algorithm[57] with a time step of 2 fs. The Lennard-Jones potential and the real part of the Coulomb interactions were truncated at 1 nm. The long-range part of the electrostatic and Lennard-Jones interactions were treated by the particle mesh Ewald method,[58,59] as implemented in GROMACS, using a relative tolerance of 10^{-5}, fourth-order cubic interpolation, and a Fourier spacing parameter of 0.12. Two stochastic velocity rescaling thermostats,[60] one for the RNA and one for the water solvent, each with a time constant of 0.1 ps, were used to control the temperature. The Berendsen barostat[61] with a time constant of 2 ps was used to control the pressure during the *NPT* runs of equilibration. The SETTLE algorithm[62] was used to constrain the TIP4P-D water geometry, and the LINCS algorithm[63] was exploited to constrain hydrogen bonds in the RNA. PLUMED 2.5[64] was used to bias the MD simulations and for the postprocessing analysis; both eRMSD and $d_{C1'-C1'}$ are implemented in PLUMED.[39]

Mono- and divalent ions are known to affect the structure and dynamics of RNA in water in such a way that, at the present date, classical force fields are still not able to capture properly.[65] To compensate for the negative charge of the single-strand RNA, in the ice simulations, we placed seven sodium (Na^+) counterions on the ice/air interface opposite the interface hosting the RNA. The charge neutralization was needed to avoid artefacts in the simulation of the inhomogeneous system by using compensating background charge and Ewald summation.[66] During the simulation time, the Na^+ ions did not cross the slab or evaporate from the interface to the other, and thus, they did not affect the structure or dynamics of the RNA. In simulations of single-

https://dx.doi.org/10.1021/acs.jpcc.0c04273
J. Phys. Chem. C XXXX, XXX, XXX−XXX

strand RNA in bulk liquid water where no inhomogeneity was present, we did not add any counterions, allowing a comparison between the bulk and ice simulations at the same (zero) ionic concentrations. As suggested in ref 65, in bulk simulation and at physiological concentrations, the number of water molecules interacting with the RNA at any instant is much larger than the number of ions, making simulations more sensitive to the water model rather than ions. Thus, for our purposes, omission of ions would not materially alter the conclusions drawn from MD runs in bulk water.

RESULTS

Figure 1a shows the free energy of CCUUCGGG single-strand RNA on ice as a function of the strand's end-to-end distance, $d_{C1'-C1'}$. A single clear minimum is found within a steep energy well, at $d_{C1'-C1'} \sim 3.2$ nm. This free energy profile is quite different from that of bulk water at 274 K (also shown in Figure 1a), where $d_{C1'-C1'}$ can more easily sample a wider range of values, that is, from ∼1.0 to 3 nm. In bulk water at 274 K, we sometimes observed $d_{C1'-C1'} < 0.5$ nm. This structure (Figure S5) originates by the π-stacking interaction of the aromatic group of the first, C, and the last, G, nucleotides. Figure 1b,c illustrates the conformation of the RNA in 274 K bulk water at $d_{C1'-C1'} \sim 1$ nm and on ice at $d_{C1'-C1'} \sim 3.2$ nm (i.e., the global minimum structure on ice), illustrating how much more extended this RNA is on ice. A side view of this global minimum structure is also shown in the profile view of Figure 1d (for clarity, ice molecules are not shown). During the course of our MD/MTD runs, the eRMSD was always greater than 1.7 (see Figure S4), both on ice and in bulk water, indicating that the RNA never explored configurations with significant base-pairing. On ice, the single-strand RNA explores a wider range of $d_{C1'-C1'}$, as shown in Figure S4c,d.

Molecular level details about the solvation of the single-strand RNA on the surface of ice are shown in Figure 2. Figure 2a shows the probability distributions of various moieties collected over the last 500 ns of the 1 μs unbiased MD simulation in the neighborhood of its global minimum structure, $d_{C1'-C1'} \sim 3.2$ nm (Figure 1c), as a function of position within the crystalline ice lattice. The origin (at 0 nm) is judged to be far enough from the air/ice interface that it represents bulk crystalline ice. For example, we note that the probability distribution for the oxygens on water molecules of ice (OW; blue curve) exhibits a symmetrical doublet at 0.4 nm, corresponding to an intact ice bilayer. As one proceeds to the right, closer to the air/ice interface, the degradation of the symmetry of these doublets indicates a transition to the QLL. The figure reveals that the phosphates (BACKBONE; orange curve) prefer to occupy positions within the bilayers centered at 1.1 nm. Ribose moieties (SUGAR; yellow curve) are seen to prefer the next bilayer, at 1.5 nm, whose degraded doublet symmetry strongly suggests a QLL structure. The bases (BASES; red) are seen to position themselves at the outermost edge of the QLL, where the density of the QLL falls off to zero. Figure 2b, a snapshot from the last part of the trajectory, is consistent with this interpretation. These results suggest that the RNA finds in the underlying crystalline structure of the ice-QLL a template that favors an extended structure, with a specific value of $d_{C1'-C1'}$. This is quite distinct from the structure characterizing single-strand RNA in bulk water, which prefers a more compressed end-to-end distance (i.e., $d_{C1'-C1'}$ in the range 1.5−3.0 nm, Figure 1a).

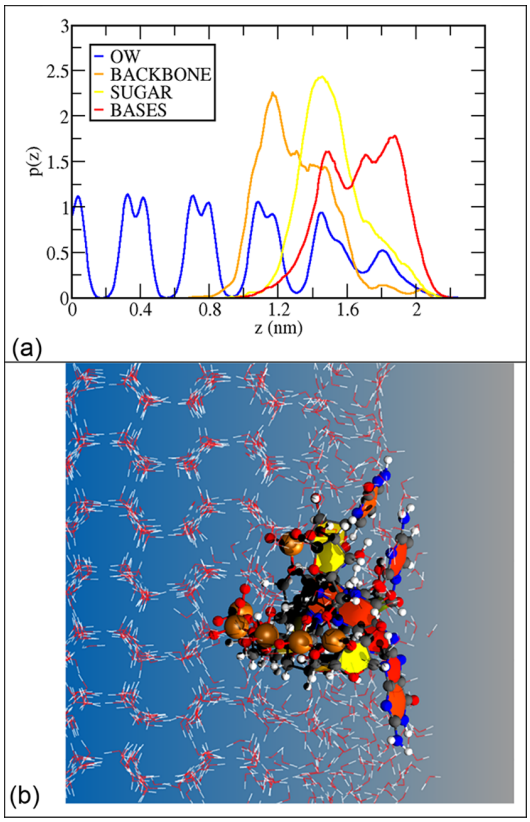

Figure 2. (a) Probability density profile as a function of the coordinate perpendicular to the ice surface (z). The probability distribution has been computed by collecting the center of mass position of water (solid blue line), phosphate backbone (orange), sugar (yellow), and bases (red) over the last 540 ns of 1 μs of MD trajectory in the global minimum. (b) Snapshot taken from the last frames of the trajectory. The underlying ice lattice is depicted via a stick model, and the single-strand RNA is depicted using a ball-and-stick model, with bases and sugar moieties superimposed as red and yellow polygons, respectively. Atoms (and the corresponding colors) are as follows: P (orange), O (red), H (white), N (blue), and C (gray).

As mentioned in the Methods section, we also performed an unbiased (i.e., without any driving potential) 1 μs MD simulation for the RNA on ice using as a starting configuration at $d_{C1'-C1'} \sim 4.4$ nm, that is, slightly stretched out from the value at the global minimum: the RNA structure on the basal air/ice interface converges to its global minimum at $d_{C1'-C1'} \sim 3.2$ nm after ∼460 ns (Figure S3a). This demonstrates the reliability of the free energy profile obtained here as a qualitative assessment of the global and local minima of different RNA structures on ice. Moreover, during the entire course of the 400 ns MTD runs, the eRMSD was found to range between 1.7 and 2.1 nm, indicating a negligible occurrence of intrastrand pairing (i.e., between bases on the RNA), as shown in Figure S4.

Figure 3 investigates the structure and kinetics of solvated single-strand RNA phosphodiesters. Figure 3a shows a snapshot of hydrogen bonding configurations of two anionic phosphodiester oxygens most deeply embedded in the ice lattice. It is evident that bonds around these oxygens are arranged in tetrahedral geometry, in which one bond is covalently bonded to phosphorus and the other three are hydrogen bonded to nearby (ice-like) water molecules. It is

https://dx.doi.org/10.1021/acs.jpcc.0c04273
J. Phys. Chem. C XXXX, XXX, XXX−XXX

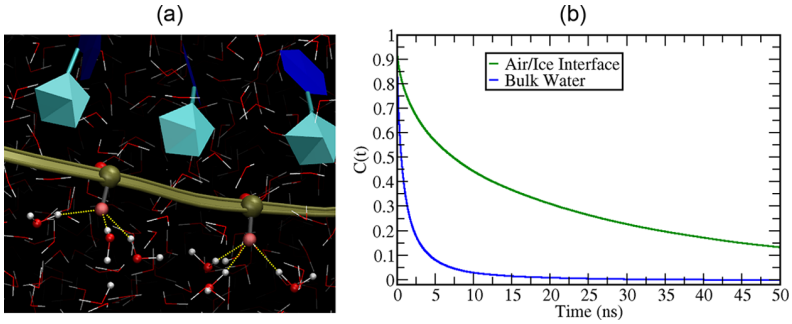

Figure 3. Hydrogen bonding between water molecules and anionic phosphate oxygens. (a) Snapshot showing hydrogen bonding interactions of two out-of-ribbon oxygens. (b) Autocorrelation functions between water molecules and phosphate groups for the solvated single-strand RNA collected over the last 350 ns of a 1 μs MD trajectory initiated at the RNA-on-ice global Gibbs energy minimum structure (green solid line) and over the last 350 ns of 700 ns run in bulk supercooled bulk water (blue solid line). For both cases, the temperature was kept at 229 K.

also evident from the figure that these interactions involve significant structuring of the solvent water—for example, all three adjacent water molecules are acting as hydrogen bond donors to the phosphodiester oxygen atoms. Statistical analysis of our RNA-on-ice MD trajectory results indicates that each phosphodiester oxygen forms 2.7 hydrogen bonds on average. It is also of interest to consider the longevity of these bonds. A hydrogen bonding autocorrelation function, $C(t)$, is shown in Figure 3b. $C(t)$ is defined as the probability of the hydrogen bond that forms between the solvent and an anionic phosphodiester oxygen remaining intact over time.[67] A comparison between the two $C(t)$ curves displayed in the figure reveals a striking difference—assuming first-order kinetics in hydrogen bond breaking and reforming,[68] the results imply an average hydrogen bond lifetime on ice of ~14 ns, compared to a lifetime of only ~1 ns in supercooled bulk water, at the same degree of supercooling.

In combination, the results shown in Figures 2 and 3 constitute compelling evidence that the anionic phosphodiester oxygens of our RNA anchor to water molecules belonging to the ice lattice underlying the QLL, rather than attaching to QLL water solvent. This is significant because anchoring of the nucleotide chain in the underlying crystalline structure would tend to lock in geometry, putting a brake on geometrical rearrangements associated with hydrolysis, and thereby favoring the maintenance of the phosphodiester link. This mechanistic brake on hydrolysis would not be operative in bulk aqueous single-strand RNA.

We turn next to what our MD results tell us about kinetic precursors of hydrolysis, as shown in Figure 4. Hydrolysis of RNA polynucleotides is initiated by attachment of the deprotonated 2′-OH group of the sugar moiety to the adjacent phosphorus atom, resulting in breakage of the phosphodiester link. The process occurs spontaneously and rapidly[69] once the 2′-OH group is deprotonated by nucleophilic attachment of the water oxygen or hydroxyl ion. Our MD simulations do not permit covalent bond formation or breakage, but they do allow us to investigate the contact frequencies of participants in this reaction. Specifically, we monitor the number of contacts between the 2′-OH hydrogen of the ribose sugar and the solvent water oxygen, defining as a contact whenever the distance, d, between water oxygen and the $H_{O2'}$ hydrogen atoms reaches 0.35 nm or less. Because such contacts must precede the hydrolysis reactions by deprotonating the 2′-OH group, we can assume that the reaction rate, r, is proportional to the number of these contacts. Although this is a crude

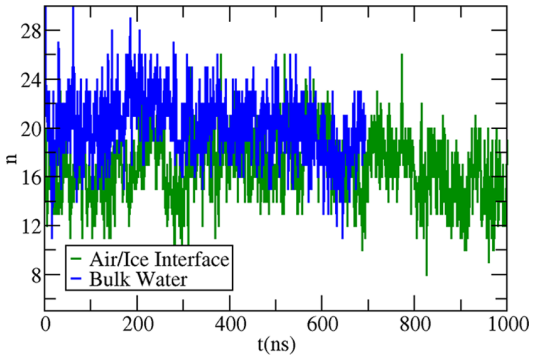

Figure 4. Number of contacts (d < 0.35 nm) between the $H_{O2'}$ hydrogen and the water oxygen as a function of time. The green solid line is the number of contacts over the 1 μs MD trajectory initiated at the RNA-on-ice global Gibbs energy minimum structure (green solid line) and the analogous curve for bulk supercooled bulk water (blue solid line). For both cases, the temperature was kept at 229 K.

approximation, it has been used successfully in the literature to provide qualitative assessment of the reaction of polyaromatic hydrocarbons and ozone on air/ice interfaces at different temperatures and reactant concentrations.[30,70] Figure 4 shows the average number of contacts (d < 0.35 nm) between the $H_{O2'}$ hydrogen and the water oxygen during the simulation of RNA on ice and in liquid water, where both are at 229 K. The average number of contacts, n, calculated over the last 350 ns of the 1 μs MD simulations of the RNA on ice and over the last 350 ns of the 700 ns MD simulations in bulk water at 229 K, are n_{ice} = 16.2 and n_{wat} = 19.6, respectively. This implies that r_{wat}/r_{ice} ~ 1.2, that is, initiation of hydrolysis would be 20% less frequent on ice compared to bulk liquid water at the same temperature (229 K).

DISCUSSION AND CONCLUSIONS

The molecular picture emerging from this work supports the view that single-strand RNA solvated on ice is more resistant to hydrolysis than its bulk aqueous counterpart. Specifically, our kinetic evidence shows that the contact between solvent water and the 2′-OH hydrogen of the ribose sugar occurs less frequently for ice-solvated RNA than for aqueous RNA at the same temperature. As this contact is an initial step in hydrolysis, it follows that hydrolysis is less likely to be initiated in ice-solvated RNA. We also find that anionic phosphodiester oxygen atoms bind preferentially with water belonging to the underlying ice lattice, in a geometry reminiscent of the strongly

https://dx.doi.org/10.1021/acs.jpcc.0c04273
J. Phys. Chem. C XXXX, XXX, XXX−XXX

kosmotropic phosphate ion (i.e., in which each anionic oxygen forms hydrogen bonds with approximately three water molecules in a tetrahedral arrangement[35,37,38]). The resulting alignment with the ice lattice confers a structural rigidity to the RNA that would, we infer, strongly resist completion of hydrolysis (among other effects). Kinetic evidence supports this inference, in that the average hydrogen bond lifetime between anionic phosphodiester oxygens and the surrounding water molecules is at least 1 order of magnitude longer for ice-solvated single-strand RNA than in the bulk aqueous solution.

Shifting focus to the "air" side of the air/ice interface, it is worth noting possible implications of solvation of hydrophobic bases in the topmost layer of the ice-QLL, exposed to (or near to) the gas phase (see Figure 2). Such exposure would make these bases more available to react with trace gases of a primordial atmosphere, compared to being fully solvated in water. Moreover, in a water-restricted environment such as the topmost layers of the air/ice interface, the bases could be more prone to base-stacking, enabling the correct base pairing with other free nucleotides located in the topmost part of the ice-QLL where the water diffusivity is faster,[71] although this is speculative. In addition, as the synthesis of building blocks for nucleotide synthesis has been shown to be plausible under prebiotic aqueous conditions,[14,72,73] an immobilized and extended RNA on ice could be more prone to polymerization and self-replication with free nucleotides diffusing in the ice-QLL than a compact arrangement, especially in the absence of protein-assisted replicase. To some extent, this was already demonstrated by the experimental findings of Deck et al.,[21] who observed the growth of daughter RNA strands from an immobilized RNA template at low temperatures.

More broadly, the idea of a "cold start" for the evolution of life on Earth has been suggested because of the reduced luminosity of the young Sun, which might have induced ice formation more extensively than thought previously.[74] In our view, the role of ice in this evolution does not preclude the role of liquid water, but rather it expands the range of possibilities in several ways. For instance, the ice-QLL itself provides diverse physicochemical properties (e.g., rigidity of the crystalline structure, water diffusivity, viscosity, and so on) as a function of depth and temperature[71,75−77] that are not obtainable in liquid water. In addition, some of the features observed here at the air/ice interface would also occur at ice/liquid interfaces within grain boundaries. Finally, as the structure of the underlying ice lattice varies greatly from facet to facet, the geometrical constraints on RNA at the air/ice interface would likely vary from those explored here. Lines of future research indicated by the results presented here include a computational first-principles MD study of phosphodiester hydrolysis and polarized second harmonic generation experiments directed at extracting detailed surface orientation information of RNA on ice surfaces.[78,79] In addition, Figure 2 highlights the fact that the phosphate group of single-strand RNA could sample different layers of the ice-QLL, suggesting that alternative or additional collective variables, other than $d_{C1'-C1'}$ or eRMSD, are needed for a more quantitative assessment of the free energy landscape of single-strand RNA on ice.

In conclusion, we have found that the air/ice interfacial environment has a distinctive impact on the orientation of surface-solvated single-strand RNA. The crystalline structure underlying the interfacial ice-QLL offers a template for immobilization of the RNA's phosphodiester groups, while its bases are exposed to the gas phase. Kinetic analysis of precursors to hydrolysis—for example, the number of contacts between water molecules and $H_{O2'}$ hydrogens of the sugar moieties—as well as structural constraints owing to the alignment of the RNA backbone with the ice lattice, indicate a resilience to hydrolysis being greater than that of supercooled bulk aqueous RNA. This work is, to the best of our knowledge, the first MD study of RNA on ice.

■ ASSOCIATED CONTENT

Supporting Information

The Supporting Information is available free of charge at https://pubs.acs.org/doi/10.1021/acs.jpcc.0c04273.

Total energy per molecule as a function of time in MD simulations of an ice I_h slab at different temperatures using the TIP4P-D model; system configurations for the TIP4P-D ice slab at different temperatures; time series of d(C1'-C1') during the (unbiased) MD simulation of single-strand RNA on ice using different configurations as the starting condition; and Scatter plots of eRMSD and the time series as a function of end-to-end C1' distance, d(C1'-C1'), during the 400 ns MTD run of single-strand RNA on the basal surface of ice and during the 100ns MTD run in bulk water (PDF)

■ AUTHOR INFORMATION

Corresponding Authors

Ivan Gladich − *International School for Advanced Studies (SISSA), 34136 Trieste, Italy; European Centre for Living Technology (ECLT), 30124 Venice, Italy;* orcid.org/0000-0003-0929-3439; Phone: +974 4454 2651; Email: igladich@hbku.edu.qa

Steven Neshyba − *Department of Chemistry, University of Puget Sound, Tacoma 98416, Washington, United States*; Phone: +1 253-879-3379; Email: nesh@pugetsound.edu

Authors

Margaret L. Berrens − *Department of Chemistry, University of Puget Sound, Tacoma 98416, Washington, United States*

Penny M. Rowe − *NorthWest Research Associates, Redmond 98052-5164, Washington, United States*

Rodolfo G. Pereyra − *Facultad de Matemática, Astronomía, Física y Computación, Universidad Nacional de Córdoba, X5000HUA Córdoba, Argentina*

Complete contact information is available at: https://pubs.acs.org/10.1021/acs.jpcc.0c04273

Author Contributions

I.G. and S.N. conceived the project. I.G., S.N., and P.M.R. wrote the manuscript. I.G. performed the MTD simulations. I.G. and R.G.P. determined the melting temperature of TIP4P-D, as reported in the Supporting Information. M.L.B., S.N., and I.G. performed unconstrained MD simulations for RNA in bulk water and on ice. All authors participated in the discussion and organization of the paper.

Notes

The authors declare no competing financial interest.

■ ACKNOWLEDGMENTS

I.G. acknowledges Dr. Sandro Bottaro, Dr. Marcelo A. Carignano, and Prof. Giovanni Bussi for insightful discussions. S.N. acknowledges seminal conversations with Peter Wim-

https://dx.doi.org/10.1021/acs.jpcc.0c04273
J. Phys. Chem. C XXXX, XXX, XXX−XXX

berger, John Hanson, Amanda Mifflin, and Babak Minofar and funding from the US National Science Foundation, CHE-1807898. S.N. and M.L.B. acknowledge support from the University of Puget Sound. P.M.R. acknowledges funding from the National Science Foundation Office of Polar Programs award 1543236.

REFERENCES

(1) Bada, J. L. New insights into prebiotic chemistry from Stanley Miller's spark discharge experiments. *Chem. Soc. Rev.* **2013**, *42*, 2186–2196.
(2) Gilbert, W. Origin of life: The RNA world. *Nature* **1986**, *319*, 618.
(3) Woese, C. R.; Dugre, D. H.; Saxinger, W. C.; Dugre, S. A. The molecular basis for the genetic code. *Proc. Natl. Acad. Sci. U.S.A.* **1966**, *55*, 966–974.
(4) Crick, F. H. C. The origin of the genetic code. *J. Mol. Biol.* **1968**, *38*, 367–379.
(5) Orgel, L. E. Evolution of the genetic apparatus. *J. Mol. Biol.* **1968**, *38*, 381–393.
(6) Robertson, M. P.; Joyce, G. F. The Origins of the RNA World. *Cold Spring Harbor Perspect. Biol.* **2012**, *4*, a003608.
(7) Abelson, J. The discovery of catalytic RNA. *Nat. Rev. Mol. Cell Biol.* **2017**, *18*, 653.
(8) Cech, T. R.; Zaug, A. J.; Grabowski, P. J. In vitro splicing of the ribosomal RNA precursor of Tetrahymena: involvement of a guanosine nucleotide in the excision of the intervening sequence. *Cell* **1981**, *27*, 487–496.
(9) Guerrier-Takada, C.; Gardiner, K.; Marsh, T.; Pace, N.; Altman, S. The RNA moiety of ribonuclease P is the catalytic submit of the enzyme. *Cell* **1983**, *35*, 849–857.
(10) Cech, T. R. A model for the RNA-catalyzed replication of RNA. *Proc. Natl. Acad. Sci. U.S.A.* **1986**, *83*, 4360.
(11) Benner, S. A.; Kim, H.-J.; Yang, Z. Setting the Stage: The History, Chemistry, and Geobiology behind RNA. *Cold Spring Harbor Perspect. Biol.* **2012**, *4*, a003541.
(12) Powner, M. W.; Gerland, B.; Sutherland, J. D. Synthesis of activated pyrimidine ribonucleotides in prebiotically plausible conditions. *Nature* **2009**, *459*, 239.
(13) Leslie E, O. Prebiotic Chemistry and the Origin of the RNA World. *Crit. Rev. Biochem. Mol. Biol.* **2004**, *39*, 99–123.
(14) Kim, S. C.; Zhou, L.; Zhang, W.; O'Flaherty, D. K.; Rondo-Brovetto, V.; Szostak, J. W. A Model for the Emergence of RNA from a Prebiotically Plausible Mixture of Ribonucleotides, Arabinonucleotides, and 2′-Deoxynucleotides. *J. Am. Chem. Soc.* **2020**, *142*, 2317–2326.
(15) Elliot, D.; Ladomery, M. *Molecular Biology of RNA*; Oxford University Press: New York, 2011.
(16) Li, Y.; Breaker, R. R. Kinetics of RNA Degradation by Specific Base Catalysis of Transesterification Involving the 2′-Hydroxyl Group. *J. Am. Chem. Soc.* **1999**, *121*, 5364–5372.
(17) Wright, T. H.; Giurgiu, C.; Zhang, W.; Radakovic, A.; O'Flaherty, D. K.; Zhou, L.; Szostak, J. W. Prebiotically Plausible "Patching" of RNA Backbone Cleavage through a 3′-5′ Pyrophosphate Linkage. *J. Am. Chem. Soc.* **2019**, *141*, 18104–18112.
(18) Vogel, S. R.; Deck, C.; Richert, C. Accelerating chemical replication steps of RNA involving activated ribonucleotides and downstream-binding elements. *Chem. Commun.* **2005**, 4922–4924.
(19) Rohatgi, R.; Bartel, D. P.; Szostak, J. W. Kinetic and Mechanistic Analysis of Nonenzymatic, Template-Directed Oligoribonucleotide Ligation. *J. Am. Chem. Soc.* **1996**, *118*, 3332–3339.
(20) Joyce, G. F. The antiquity of RNA-based evolution. *Nature* **2002**, *418*, 214.
(21) Deck, C.; Jauker, M.; Richert, C. Efficient enzyme-free copying of all four nucleobases templated by immobilized RNA. *Nat. Chem.* **2011**, *3*, 603.
(22) Attwater, J.; Wochner, A.; Holliger, P. In-ice evolution of RNA polymerase ribozyme activity. *Nat. Chem.* **2013**, *5*, 1011.
(23) Hub, J. S.; Caleman, C.; van der Spoel, D. Organic molecules on the surface of water droplets—an energetic perspective. *Phys. Chem. Chem. Phys.* **2012**, *14*, 9537–9545.
(24) Habartová, A.; Valsaraj, K. T.; Roeselová, M. Molecular Dynamics Simulations of Small Halogenated Organics at the Air-Water Interface: Implications in Water Treatment and Atmospheric Chemistry. *J. Phys. Chem. A* **2013**, *117*, 9205–9215.
(25) Bartels-Rausch, T.; Jacobi, H.-W.; Kahan, T. F.; Thomas, J. L.; Thomson, E. S.; Abbatt, J. P. D.; Ammann, M.; Blackford, J. R.; Bluhm, H.; Boxe, C.; Domine, F.; Frey, M. M.; Gladich, I.; Guzmán, M. I.; Heger, D.; Huthwelker, T.; Klán, P.; Kuhs, W. F.; Kuo, M. H.; Maus, S.; Moussa, S. G.; McNeill, V. F.; Newberg, J. T.; Pettersson, J. B. C.; Roeselová, M.; Sodeau, J. R. A review of air-ice chemical and physical interactions (AICI): liquids, quasi-liquids, and solids in snow. *Atmos. Chem. Phys.* **2014**, *14*, 1587–1633.
(26) Gladich, I.; Pfalzgraff, W.; Maršálek, O.; Jungwirth, P.; Roeselová, M.; Neshyba, S. Arrhenius analysis of anisotropic surface self-diffusion on the prismatic facet of ice. *Phys. Chem. Chem. Phys.* **2011**, *13*, 19960–19969.
(27) Kahan, T. F.; Donaldson, D. J. Photolysis of polycyclic aromatic hydrocarbons on water and ice surfaces. *J. Phys. Chem. A* **2007**, *111*, 1277–1285.
(28) Kahan, T. F.; Donaldson, D. J. Heterogeneous ozonation kinetics of phenanthrene at the air-ice interface. *Environ. Res. Lett.* **2008**, *3*, 045006.
(29) Ardura, D.; Kahan, T. F.; Donaldson, D. J. Self-Association of Naphthalene at the Air–Ice Interface. *J. Phys. Chem. A* **2009**, *113*, 7353–7359.
(30) Liyana-Arachchi, T. P.; Valsaraj, K. T.; Hung, F. R. Molecular Simulation Study of the Adsorption of Naphthalene and Ozone on Atmospheric Air/Ice Interfaces. *J. Phys. Chem. A* **2011**, *115*, 9226–9236.
(31) Michaelides, A.; Slater, B. Melting the ice one layer at a time. *Proc. Natl. Acad. Sci. U.S.A.* **2017**, *114*, 195.
(32) Smit, W. J.; Bakker, H. J. The Surface of Ice Is Like Supercooled Liquid Water. *Angew. Chem., Int. Ed.* **2017**, *56*, 15540–15544.
(33) Ram, K.; Anastasio, C. Photochemistry of phenanthrene, pyrene, and fluoranthene in ice and snow. *Atmos. Environ.* **2009**, *43*, 2252–2259.
(34) Sánchez, M. A.; Kling, T.; Ishiyama, T.; van Zadel, M.-J.; Bisson, P. J.; Mezger, M.; Jochum, M. N.; Cyran, J. D.; Smit, W. J.; Bakker, H. J.; Shultz, M. J.; Morita, A.; Donadio, D.; Nagata, Y.; Bonn, M.; Backus, E. H. G. Experimental and theoretical evidence for bilayer-by-bilayer surface melting of crystalline ice. *Proc. Natl. Acad. Sci. U.S.A.* **2017**, *114*, 227.
(35) Moelbert, S.; Normand, B.; De Los Rios, P. Kosmotropes and chaotropes: modelling preferential exclusion, binding and aggregate stability. *Biophys. Chem.* **2004**, *112*, 45–57.
(36) Dill, K. A.; Truskett, T. M.; Vlachy, V.; Hribar-Lee, B. Modeling Water, the Hydrophobic Effect, and Ion Solvation. *Annu. Rev. Biophys. Biomol. Struct.* **2005**, *34*, 173–199.
(37) Chen, C.; Huang, C.; Waluyo, I.; Weiss, T.; Pettersson, L. G. M.; Nilsson, A. Long-range ion-water and ion-ion interactions in aqueous solutions. *Phys. Chem. Chem. Phys.* **2015**, *17*, 8427–8430.
(38) Sharma, B.; Chandra, A. Ab Initio Molecular Dynamics Simulation of the Phosphate Ion in Water: Insights into Solvation Shell Structure, Dynamics, and Kosmotropic Activity. *J. Phys. Chem. B* **2017**, *121*, 10519–10529.
(39) Bottaro, S.; Banáš, P.; Šponer, J.; Bussi, G. Free Energy Landscape of GAGA and UUCG RNA Tetraloops. *J. Phys. Chem. Lett.* **2016**, *7*, 4032–4038.
(40) Cesari, A.; Bottaro, S.; Lindorff-Larsen, K.; Banáš, P.; Šponer, J.; Bussi, G. Fitting Corrections to an RNA Force Field Using Experimental Data. *J. Chem. Theory Comput.* **2019**, *15*, 3425–3431.
(41) Tan, D.; Piana, S.; Dirks, R. M.; Shaw, D. E. RNA force field with accuracy comparable to state-of-the-art protein force fields. *Proc. Natl. Acad. Sci. U.S.A.* **2018**, *115*, E1346–E1355.

https://dx.doi.org/10.1021/acs.jpcc.0c04273
J. Phys. Chem. C XXXX, XXX, XXX–XXX

(42) Robustelli, P.; Piana, S.; Shaw, D. E. Developing a molecular dynamics force field for both folded and disordered protein states. *Proc. Natl. Acad. Sci. U.S.A.* **2018**, *115*, E4758−E4766.
(43) Piana, S.; Donchev, A. G.; Robustelli, P.; Shaw, D. E. Water dispersion interactions strongly influence simulated structural properties of disordered protein states. *J. Phys. Chem. B* **2015**, *119*, 5113−5123.
(44) Abascal, J. L. F.; Vega, C. A general purpose model for the condensed phases of water: TIP4P/2005. *J. Chem. Phys.* **2005**, *123*, 234505.
(45) Vega, C.; Abascal, J. L. F. Simulating water with rigid non-polarizable models: a general perspective. *Phys. Chem. Chem. Phys.* **2011**, *13*, 19663−19688.
(46) Vega, C.; Abascal, J. L. F.; Conde, M. M.; Aragones, J. L. What ice can teach us about water interactions: a critical comparison of the performance of different water models. *Faraday Discuss.* **2009**, *141*, 251−276.
(47) Buch, V.; Sandler, P.; Sadlej, J. Simulations of H2O solid, liquid, and clusters, with an emphasis on ferroelectric ordering transition in hexagonal ice. *J. Phys. Chem. B* **1998**, *102*, 8641−8653.
(48) Muchová, E.; Gladich, I.; Picaud, S.; Hoang, P. N. M.; Roeselova, M. The Ice-Vapor Interface and the Melting Point of Ice I(h) for the Polarizable POL3 Water Model. *J. Phys. Chem. A* **2011**, *115*, 5973−5982.
(49) Conde, M. M.; Vega, C.; Patrykiejew, A. The thickness of a liquid layer on the free surface of ice as obtained from computer simulation. *J. Chem. Phys.* **2008**, *129*, 014702.
(50) Gladich, I.; Roeselová, M. Comparison of selected polarizable and nonpolarizable water models in molecular dynamics simulations of ice Ih. *Phys. Chem. Chem. Phys.* **2012**, *14*, 11371−11385.
(51) Barducci, A.; Bussi, G.; Parrinello, M. Well-Tempered Metadynamics: A Smoothly Converging and Tunable Free-Energy Method. *Phys. Rev. Lett.* **2008**, *100*, 020603.
(52) Branduardi, D.; Bussi, G.; Parrinello, M. Metadynamics with Adaptive Gaussians. *J. Chem. Theory Comput.* **2012**, *8*, 2247−2254.
(53) Kührová, P.; Banáš, P.; Best, R. B.; Šponer, J.; Otyepka, M. Computer Folding of RNA Tetraloops? Are We There Yet? *J. Chem. Theory Comput.* **2013**, *9*, 2115−2125.
(54) Bergonzo, C.; Henriksen, N. M.; Roe, D. R.; Cheatham, T. E., 3rd Highly sampled tetranucleotide and tetraloop motifs enable evaluation of common RNA force fields. *RNA* **2015**, *21*, 1578−1590.
(55) Bottaro, S.; Di Palma, F.; Bussi, G. The role of nucleobase interactions in RNA structure and dynamics. *Nucleic Acids Res.* **2014**, *42*, 13306−13314.
(56) Abraham, M. J.; Murtola, T.; Schulz, R.; Páll, S.; Smith, J. C.; Hess, B.; Lindahl, E. GROMACS: High performance molecular simulations through multi-level parallelism from laptops to supercomputers. *SoftwareX* **2015**, *1−2*, 19−25.
(57) Hockney, R. W.; Goel, S. P.; Eastwood, J. W. Quiet High-Resolution Computer Models of a Plasma. *J. Comput. Phys.* **1974**, *14*, 148−158.
(58) Darden, T.; York, D.; Pedersen, L. Particle Mesh Ewald-An N.Log(N) Method for Ewald Sums in Large Systems. *J. Chem. Phys.* **1993**, *98*, 10089−10092.
(59) Essmann, U.; Perera, L.; Berkowitz, M. L.; Darden, T.; Lee, H.; Pedersen, L. G. A Smooth Particle Mesh Ewald Method. *J. Chem. Phys.* **1995**, *103*, 8577−8593.
(60) Bussi, G.; Donadio, D.; Parrinello, M. Canonical sampling through velocity rescaling. *J. Chem. Phys.* **2007**, *126*, 014101.
(61) Berendsen, H. J. C.; Postma, J. P. M.; van Gunsteren, W. F.; Dinola, A.; Haak, J. R. Molecular Dynamics With Coupling To An External Bath. *J. Chem. Phys.* **1984**, *81*, 3684−3690.
(62) Miyamoto, S.; Kollman, P. A. SETTLE—An Analytical Version of the SHAKE and RATTLE Algorithm for Rigid Water Models. *J. Comput. Chem.* **1992**, *13*, 952−962.
(63) Hess, B.; Bekker, H.; Berendsen, H. J. C.; Fraaije, J. G. E. M. LINCS: A linear constraint solver for molecular simulations. *J. Comput. Chem.* **1997**, *18*, 1463−1472.
(64) Tribello, G. A.; Bonomi, M.; Branduardi, D.; Camilloni, C.; Bussi, G. PLUMED 2: New feathers for an old bird. *Comput. Phys. Commun.* **2014**, *185*, 604−613.
(65) Šponer, J.; Bussi, G.; Krepl, M.; Banáš, P.; Bottaro, S.; Cunha, R. A.; Gil-Ley, A.; Pinamonti, G.; Poblete, S.; Jurečka, P.; Walter, N. G.; Otyepka, M. RNA Structural Dynamics As Captured by Molecular Simulations: A Comprehensive Overview. *Chem. Rev.* **2018**, *118*, 4177−4338.
(66) Hub, J. S.; de Groot, B. L.; Grubmüller, H.; Groenhof, G. Quantifying Artifacts in Ewald Simulations of Inhomogeneous Systems with a Net Charge. *J. Chem. Theory Comput.* **2014**, *10*, 381−390.
(67) Luzar, A.; Chandler, D. Effect of Environment on Hydrogen Bond Dynamics in Liquid Water. *Phys. Rev. Lett.* **1996**, *76*, 928−931.
(68) Luzar, A. Resolving the hydrogen bond dynamics conundrum. *J. Chem. Phys.* **2000**, *113*, 10663−10675.
(69) Voet, D.; Voet, J. G. *Biochemistry*; Wiley & Sons: New York, 2011.
(70) Vácha, R.; Cwiklik, L.; Řezáč, J.; Hobza, P.; Jungwirth, P.; Valsaraj, K.; Bahr, S.; Kempter, V. Adsorption of Aromatic Hydrocarbons and Ozone at Environmental Aqueous Surfaces. *J. Phys. Chem. A* **2008**, *112*, 4942−4950.
(71) Louden, P. B.; Gezelter, J. D. Why is Ice Slippery? Simulations of Shear Viscosity of the Quasi-Liquid Layer on Ice. *J. Phys. Chem. Lett.* **2018**, *9*, 3686−3691.
(72) Powner, M. W.; Gerland, B.; Sutherland, J. D. Synthesis of activated pyrimidine ribonucleotides in prebiotically plausible conditions. *Nature* **2009**, *459*, 239−242.
(73) Becker, S.; Feldmann, J.; Wiedemann, S.; Okamura, H.; Schneider, C.; Iwan, K.; Crisp, A.; Rossa, M.; Amatov, T.; Carell, T. Unified prebiotically plausible synthesis of pyrimidine and purine RNA ribonucleotides. *Science* **2019**, *366*, 76.
(74) Bada, J. L.; Lazcano, A. ORIGIN OF LIFE: Some Like It Hot, But Not the First Biomolecules. *Science* **2002**, *296*, 1982.
(75) Wei, X.; Miranda, P. B.; Shen, Y. R. Surface vibrational spectroscopic study of surface melting of ice. *Phys. Rev. Lett.* **2001**, *86*, 1554−1557.
(76) Bartels-Rausch, T.; Orlando, F.; Kong, X.; Artiglia, L.; Ammann, M. Experimental Evidence for the Formation of Solvation Shells by Soluble Species at a Nonuniform Air-Ice Interface. *ACS Earth Space Chem.* **2017**, *1*, 572−579.
(77) Gladich, I.; Oswald, A.; Bowens, N.; Naatz, S.; Rowe, P.; Roeselova, M.; Neshyba, S. Mechanism of anisotropic surface self-diffusivity at the prismatic ice-vapor interface. *Phys. Chem. Chem. Phys.* **2015**, *17*, 22947−22958.
(78) Tran, R. J.; Sly, K. L.; Conboy, J. C. Applications of Surface Second Harmonic Generation in Biological Sensing. *Annu. Rev. Anal. Chem.* **2017**, *10*, 387−414.
(79) Birman, Y.; Khorsand, S.; Tu, E.; Mortensen, R. B.; Butko, M. T. Second-harmonic generation-based methods to detect and characterize ligand-induced RNA conformational changes. *Methods* **2019**, *167*, 92−104.
(80) Laio, A.; Rodriguez-Fortea, A.; Gervasio, F. L.; Ceccarelli, M.; Parrinello, M. Assessing the Accuracy of Metadynamics. *J. Phys. Chem. B* **2005**, *109*, 6714−6721.
(81) Tiwary, P.; Parrinello, M. A Time-Independent Free Energy Estimator for Metadynamics. *J. Phys. Chem. B* **2015**, *119*, 736−742.

https://dx.doi.org/10.1021/acs.jpcc.0c04273
J. Phys. Chem. C XXXX, XXX, XXX−XXX